# Identification of the Active Cu Phase in the Water−Gas Shift Reaction over Cu/ZrO₂ from First Principles

## Qian-Lin Tang and Zhi-Pan Liu*

*Shanghai Key Laboratory of Molecular Catalysis and Innovative Materials, Department of Chemistry, Key Laboratory of Computational Physical Science (Ministry of Education), Fudan University, Shanghai 200433, China*

The water−gas shift (WGS) reaction ($H_2O + CO \rightarrow H_2 + CO_2$) is regarded as a key catalytic process in a future hydrogen economy. In this report, first-principles density functional theory (DFT) calculations have been utilized to identify the WGS mechanism over a Cu/oxide model catalyst, Cu/ZrO₂. The catalytic reaction is found to occur at the Cu sites that are in the vicinity of Cu/oxides interfaces, where the Cu electronic structure is markedly modified by the oxygen-rich Cu/oxides interface. DFT-based microkinetic modeling further shows that a COOH-involved mechanism is responsible for the WGS reaction, with the H₂O dissociation step being rate-controlling. By comparing the reaction thermodynamics and kinetics over three systems, namely, Cu/ZrO₂, unsupported Cu strip, and Cu(111), we demonstrate that positively charged Cu clusters afford much enhanced catalytic activity in H₂O dissociation. The ZrO₂ support acts as a charge buffer to accept/release electrons from/to the Cu particle. The oxygen-rich metal-oxide interface, although not directly involved in catalysis, acts as a key promoter in enhancing catalytic activity in Cu-based catalysis.

## 1. Introduction

Oxide-supported copper is an important type of heterogeneous catalyst, which is widely applied in industry for processes such as methanol synthesis and the water−gas shift (WGS) reaction.[1,2] In general, the composite catalysts exhibit higher activity than the individual component.[3,4] For example, recent studies of the WGS reaction over metal-oxide catalysts by Rodríguez and co-workers have clearly shown that the oxide does play a positive role in promoting this reaction.[5−7] The so-called synergetic effect is however not well understood at the atomic level, not at least because of the complexity of the catalytic process under realistic conditions. While it is no doubt that the oxide support directly participates in making/breaking chemical bonds for some reactions,[8] such as methanol synthesis from CO or CO₂ hydrogenation over Cu/ZrO₂,[9] the active sites of many other reactions, the WGS reaction for example, are less certain, and the catalytic role of the oxide support is often subject to debate.

For its significance in making and purifying hydrogen, the WGS reaction over Cu-based catalysts has been intensively investigated, mainly focusing on the reaction mechanism and the chemical nature of the active site.[10,11] To date, two reaction routes have often been suggested, namely, a regenerative redox mechanism and an intermediate-mediated mechanism.[10−18] The former features the $CO^* + O^* \rightarrow CO_2 + 2^*$ elementary step (an asterisk indicates a surface vacant site), with the adsorbed CO being oxidized straightforwardly by the atomic oxygen that is produced from H₂O dissociation. On the other hand, the latter is named after the carbon-containing surface intermediates (e.g., formate, carboxyl, and carbonate), which are formed presumably via the coupling between CO and a kind of surface species (e.g., H and OH). Both mechanisms share a common elementary step, the dissociative adsorption of water ($H_2O^* + ^* \rightarrow OH^* + H^*$), which is generally believed to be the rate-determining step.[12,13,17−19]

Theoretically, the redox mechanism and the associative carboxyl (COOH) mechanism have been explored on pure Cu surfaces/clusters with DFT calculations.[3,20−22] It was suggested that the redox route is preferable on Cu(100),[20] while the carboxyl route is the dominant path on Cu(111)[21,22] and a Cu₂₉ cluster.[3,20]

As for the active sites of the WGS reaction, a key issue is to clarify whether charged copper sites are in fact catalytically more relevant.[10] It is known that pure Cu alone is active for the WGS reaction, as shown by Campbell and co-workers,[17,18,23] although the catalytic activity measured is not high.[3,24] Several recent DFT calculations[20−22] confirmed that the WGS reaction can indeed occur on clean Cu(100) and Cu(111) surfaces. In line with this, many other groups proposed that metallic Cu is the active center even for the Cu/oxide composite systems.[18,25−28] Recent time-resolved in situ X-ray diffraction studies even claimed that metallic Cu is the only stable species in these systems under reaction conditions.[29,30] However, this view meets difficulties to explain why the variation of the oxide supports will affect the rate of the WGS reaction markedly, as reported by a large volume of experimental studies.[2,3,5−7,11,24,29,31−34] In particular, the specific activity of Cu/ZrO₂ is found to be higher than that of Cu supported on other oxides such as Al₂O₃, ZnO/Al₂O₃, and SiO₂.[2,15] X-ray photoelectron spectroscopy suggested that highly dispersed metallic Cu can be readily oxidized to Cu⁺ and Cu²⁺ under realistic reaction conditions.[35] It was therefore implied that the positively charged Cu supported on oxides may be the real active site in Cu/ZrO₂ and Cu/ZnO catalysts.[15,16,33]

Obviously, the first-principles simulation on a composite Cu/oxide system could be a desirable tool to resolve the puzzles on the mechanism and the active sites. This is, however, rather challenging because the structure of the composite system is not known exactly at the atomic level, and a full-scale simulation including both nanosized metal particles and the oxide support is too demanding in computation. In this work, we aim to go further to understand the support effect by exploring the possible

* To whom correspondence should be addressed. Fax: (+86) 21-6564-2400; E-mail: zpliu@fudan.edu.cn.

**8424** *J. Phys. Chem. C, Vol. 114, No. 18, 2010*

Tang and Liu

WGS reaction channels over a binary composite Cu/ZrO$_2$ model system, where a two-layer close-packed Cu strip is loaded onto the ZrO$_2$ oxide. To validate the findings from our model Cu/oxide system, the reactions on the unsupported Cu strip and Cu(111) were performed in parallel, and the results were compared in terms of kinetics to identify the catalytic role of oxides. While our results confirm that the WGS reaction takes places exclusively on Cu sites, not at the Cu/oxide interface, the presence of oxide is shown to significantly speed up the key elementary reaction step, that is, H$_2$O dissociation. We suggest that the catalytic conversion occurs dominantly at the Cu sites in the vicinity of the Cu/oxide interface, where the Cu is partially oxidized.

## 2. Slab Models and DFT Setups

All of the periodic DFT calculations have been performed with the SIESTA package.[36] The utilized exchange-correlation functional was at the level of the Perdew−Burke−Ernzerf (PBE) flavor of the generalized gradient approximation (GGA).[37] The interaction between atomic cores and valence electrons was described by the Troullier−Martins norm-conserving pseudopotentials.[38] The semicore states of Zr atoms, $4s^2 4p^6$, were also treated as the valence states. A numerical atomic orbital basis set of the double-$\xi$ plus polarization was utilized, with a radii confinement of the orbitals equivalent to an energy shift of 0.01 eV.[39] The kinetic energy cutoff for the real-space mesh employed to represent the density was specified to be 150 Ry. The first Brillouin zone of the slabs was sampled using a (4 × 6 × 1) Monkhorst−Pack grid[40] for Cu(111) p(3 × 2) supercells and using only the Γ-point for other large supercells involving Cu strips. Geometry optimization was implemented with the quasi-Newton Broyden method until all of the remaining forces acting on each relaxed coordinates were below 0.1 eV/Å. Transition states (TSs) of all of the catalytic reactions were searched with our recently developed constrained Broyden minimization method.[41] The TSs were identified when (i) the forces on the atoms diminished and (ii) the energy was a maximum along the reaction coordinate but a minimum with respect to other degrees of freedom. Vibrational frequencies were computed by diagonalizing the Hessian matrix, which was constructed numerically using the finite difference method with the step size of ±0.02 Å along each Cartesian coordinate. Convergence of reported reaction energies and barriers was verified with regard to the basis set, energy shift, and kinetic energy cutoff. By including the zero-point energy (ZPE) correction (0.13 eV) and the temperature dependence of enthalpy from 0 to 573 K (−0.01 eV),[42] the reaction heat of the WGS reaction was predicted to be exothermic by −0.77 eV at 573 K and 1 bar with the above DFT setups (experimental value, −0.43 eV).[10]

The Cu/ZrO$_2$ system in our modeling is created by anchoring a two-layer thick (111)-like copper strip onto a stepped ($\bar{2}$12) surface of monoclinic ZrO$_2$ (Figure 1a), which has been utilized previously for studying the CO$_2$ hydrogenation reaction at the Cu/ZrO$_2$ interface.[43] The reason to select such a model is based on the facts that (i) Cu particles were highly dispersed on ZrO$_2$ (even one metal monolayer was observed experimentally)[15,34] and (ii) ZrO$_2$($\bar{2}$12) is a commonly exposed defected facet of ZrO$_2$,[44] and it also provides a better anchoring site for metals than the most stable ($\bar{1}$11) facet.[43,45] It is necessary to mention that this Cu/ZrO$_2$ structure simulated was already utilized in our recent study for CO$_2$ hydrogenation occurring over Cu/ZrO$_2$, which was shown to be able to capture the chemistry of the interface.[43] A three-layer thick slab with a p(3 × 1) large unit
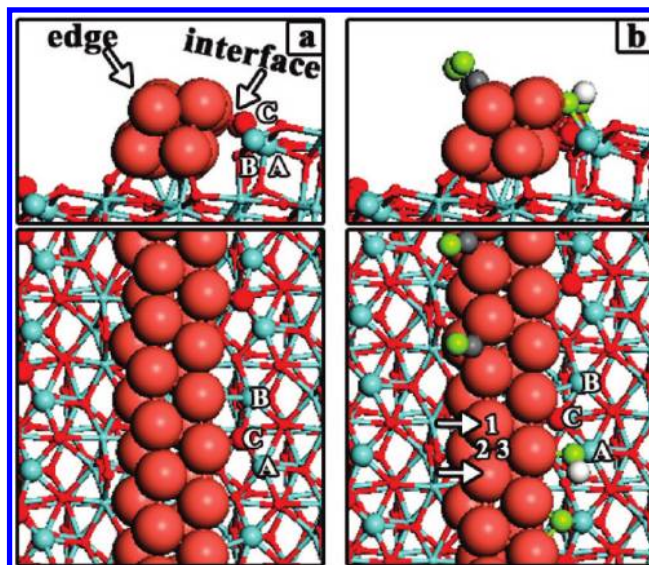


**Figure 1.** Optimized structures of (a) a Cu strip on the stepped ($\bar{2}$12) surface of monoclinic ZrO$_2$ and (b) the Cu/ZrO$_2$ model system where the Cu−ZrO$_2$($\bar{2}$12) interface is occupied by O and OH and the Cu strip is precovered by extra CO. The meanings of the labels are as follows: A, six-coordinated Zr; B, five-coordinated Zr; C, two-coordinated lattice O. The upper panels are the side view, and the lower panels are the top view. The adsorption/reaction sites investigated in the work are at the edge-Cu atoms, as indicated by the arrows as follows: 1, top; 2, bridge; 3, fcc. H, white; C, gray; O of adsorbates, light green; lattice O, red; Cu, orange; Zr, cyan.

cell (20.44 Å × 11.69 Å) was employed to represent the ($\bar{2}$12) surface to ensure a good lattice match with the loaded Cu strip. The topmost 24 ZrO$_2$ formula units as well as all surface species were allowed to be fully relaxed, while the remaining 30 ZrO$_2$ units were frozen in the bulk truncated positions. The presence of surface oxygen vacancies was not taken into account here because ZrO$_2$ is known to be irreducible under reaction conditions.[46] In order to elucidate the support effect, comparative studies on other two different kinds of pure Cu substrates were also performed, (i) the unsupported Cu strip that is created by removing the oxide support from the above Cu/ZrO$_2$ model, where the exposed Cu atoms are six- and seven-coordinated (Figure 1) and (ii) the Cu(111) surface, where the surface Cu is nine-coordinated. The Cu(111) surface is represented by a four-layer thick slab of a p(3 × 2) periodicity (7.696 Å × 5.131 Å), with the top two layers relaxed. Two neighboring slabs are separated by a vacuum spacing of 16 Å. The energies of all gas-phase species were calculated by using a 16 Å$^3$ cubic unit cell.

## 3. Results and Discussion

**3.1. Interface Characteristics and Oxygen-Rich Cu/ZrO$_2$ Model System.** In this work, the adsorption/binding energy of an adsorbate X, $E_{ad}(X)$, was defined as $E_{ad}(X) = E_{substrate} + E_X - E_{X/substrate}$, where $E$ is the DFT total energy and a positive $E_{ad}(X)$ represents an exothermic adsorption process. From our calculations, the binding energy of a Cu adatom at ZrO$_2$($\bar{2}$12) is 1.08 eV, less than one-third of the calculated cohesive energy of bulk Cu, 3.55 eV (experimental value, 3.49 eV[47]). This reveals that the growth of metallic Cu particles over the oxide surface is favored thermodynamically, which is in agreement with the observation by transmission electron microscopy on Cu/oxides catalysts.[48] Our optimized Cu strip deposited on ZrO$_2$ is shown in Figure 1a. The Cu/ZrO$_2$ interface and the edge of deposited Cu expose only the lowest-surface-energy facets of the indi-

vidual components, that is, the ($\bar{1}$11) terrace of $ZrO_2$ and the Cu(111) surface, which guarantees the structures to be energetically stable during reaction. We found that the Cu strip interacts mainly with the surface Os of $ZrO_2$, with the newly formed Cu−O bonds being typically about 2.1 Å. The strength of each Cu−O bond is estimated to be 0.71 eV on average (i.e., adsorption energy of the Cu strip divided by number of Cu−O bonds). The interface between the oxide step edge and the Cu strip can be viewed as an array of $(Zr)_2$−O−Cu linkages (see Figure 1a), where the O is the original two-coordinated lattice O ($O_{2c}$) at the step edge and the two Zr atoms are five-coordinated ($Zr_{5c}$) and six-coordinated ($Zr_{6c}$) lattice Zr.

Once the $Cu/ZrO_2$ model system is established, it is possible to determine where the catalytic active site for the WGS reaction is. We have first considered the adsorption of reactants CO and $H_2O$ in the model system. We found that CO adsorbs preferentially on pure Cu sites; the adsorption energy is 1.33 eV at the Cu sites next to the interface Cu, which is 0.25 eV larger than the value at the interfacial Cu and 0.56 eV larger than that on the $Zr_{5c}$ site of $ZrO_2$. However, $H_2O$ favors sitting on $ZrO_2$ sites of the $Cu/ZrO_2$ interface with $E_{ad}(H_2O) = 0.72$ eV, which is ∼0.3 eV larger than that for $H_2O$ adsorption on Cu-only sites.

Since CO adsorbs dominantly on Cu sites, the active sites for the WGS reaction are either the interfacial sites involving both Cu and $ZrO_2$ or the pure Cu sites. Since the metal-oxide interface is known to be highly active for many heterogeneous reactions,[8] we first examined whether CO can be directly oxidized by the oxidative species, including OH and O, at the interfacial sites of $Cu/ZrO_2$. These recombination reactions, namely, CO* + O* → $CO_2$ + 2* and CO* + OH* → COOH* + *, are the key steps in the WGS reaction. At the initial state, the O and OH adsorb at the interface by forming bonding with not only the $Zr_{5c}$ but also the neighboring interfacial Cu atoms, whereas CO adsorbs at its most stable Cu sites. The TSs have been identified with the nascent C−O bonds being 1.80 and 1.76 Å for CO* + O* → $CO_2$ + 2* and CO* + OH* → COOH* + *, respectively. Importantly, we found that the two reactions are strongly endothermic by 1.0 eV, and consistently, these reactions are hindered by high barriers of at least 1.39 eV. Since the barriers are even higher than the adsorption energy of CO and the oxidization is highly endothermic, it implies that CO can hardly be oxidized by the interfacial oxygen species.

Apparently, the difficulty in CO oxidation at the interface can be attributed to the large affinities of O and OH at the interfacial sites; the O and OH at the interface are 1.32 and 0.69 eV more stable than those on the Cu strip. It might be interesting to mention that CO oxidation has been calculated on $Au/TiO_2$[49] and $Au/ZrO_2$[45] interfaces in our previous work. The CO + $O_2$ and CO + O reactions can occur facilely at the interface with low barriers (below 0.5 eV), which is understandable as the Au−O bonds are much weaker than the Cu−O bonds. From the above calculations, we would expect that the OH and O species that are available from $H_2O$ dissociation (the dissociation barrier of $H_2O$ at the $Cu/ZrO_2$ interface is below 0.50 eV[43]) will occupy first the active $Cu/ZrO_2$ interface sites, and they are reluctant to react with CO under reaction conditions. Naturally, an oxygen-rich interface will be formed in situ and thus cause the Cu sites near the interface to be partly oxidized during the WGS reaction. The finding is in line with Auger electron spectra of the Cu/ZnO catalyst where $Cu^+$ at the Cu/oxide boundary is identified.[33]

On the basis of the above preliminary calculations, we then terminated the interface sites of the $Cu/ZrO_2$ system by adding extra O and OH species, and this more realistic oxygen-rich

**TABLE 1: Adsorption Sites, Selected Adsorbate (A)−Cu Bond Length (Unit: Å), and Binding Energy $E_{ad}$ (Unit: eV) for Possible Species Involved in the WGS Reaction at the Cu Edge of $Cu/ZrO_2$[a]**

| species | ads. site | A−Cu | $d_{A-Cu}$ | $E_{ad}$ | $E_{ad}^{Cu_{us}}$ | $E_{ad}^{Cu(111)}$ |
|---|---|---|---|---|---|---|
| H | fcc | H−Cu | 1.67/1.76/1.80 | 2.46 | 2.01 | 2.43 |
| O | fcc | O−Cu | 1.86/1.92/1.94 | 2.25 | 0.87 | 1.44 |
| OH | bri | O−Cu | 1.98/1.99 | 3.55 | 3.04 | 3.08 |
| CO | bri | C−Cu | 1.94/2.00 | 1.33 | 0.93 | 1.06 |
| $H_2$ | top | H−Cu | 3.20/3.21 | 0.00 | 0.02 | 0.02 |
| $H_2O$ | top | O−Cu | 2.23 | 0.25 | 0.29 | 0.24 |
| $CO_2$ | top | C−Cu | 3.20 | 0.06 | 0.07 | 0.10 |
|  |  | O−Cu | 3.06/3.75 |  |  |  |
| *cis*-COOH | top | C−Cu | 1.94 | 2.41 | 1.85 | 1.89 |
|  |  | O−Cu | 2.09 |  |  |  |
| *trans*-COOH | top | C−Cu | 1.94 | 2.32 | 1.71 | 1.79 |
|  |  | O−Cu | 2.06 |  |  |  |
| HCOO | top | O−Cu | 1.97/1.99 | 3.29 | 2.80 | 2.83 |

[a] Adsorption energy of each species on $Cu_{us}$, $E_{ad}^{Cu_{us}}$ and on Cu(111), $E_{ad}^{Cu(111)}$, are also listed for comparison. The adsorption energy of O is computed with respect to $1/2$ $O_2$ in the gas phase.

$Cu/ZrO_2$ system was then utilized as our model catalyst for the further investigation of the WGS reaction mechanism. Considering that the reaction occurs on the Cu sites where 16 exposed Cu surface atoms are available in the model unit cell, we also added three CO molecules per unit cell as the preadsorbed species to model a local coverage of adsorbate of ∼0.25 monolayer (ML) (Figure 1b) for a fair comparison with previous DFT calculations on (111) surfaces where a 0.25 ML in a p(2 × 2) structure was usually utilized.[21,22] It should be mentioned that there is no direct bond sharing between the preadsorbed CO and the reaction intermediates in our modeling of the WGS reaction. In the oxygen-rich $Cu/ZrO_2$ system, the Cu strip is positively charged by 2.90 |e| according to our Bader charge analysis,[50,51] which is due to the donation of electrons from Cu to the oxide lattice O and the extra oxidative species at the interface.

In the following, our results on the reaction mechanism will first be elaborated, and the catalytic role of oxide support in the WGS reaction will then be analyzed based on the microkinetic simulation.

**3.2. Mechanism of the WGS Reaction with and without the $ZrO_2$ Support.** Before the investigation of the WGS reaction mechanism, it is essential to map out the potential energy surface (PES) of reaction intermediates at the Cu sites in the $Cu/ZrO_2$ model system. We have considered nine key species, namely, H, O, OH, CO, $H_2$, $H_2O$, $CO_2$, COOH, and HCOO. The binding energies and the geometrical parameters of the most stable adsorption states for the species are summarized in Table 1, and the corresponding adsorption configurations are illustrated in Figure 2. We found that CO and OH prefer to adsorb at the edge-bridge sites of the Cu strip, and the unsaturated H and O species tend to sit at the three-fold fcc sites. It is noted that the PES of CO and OH on Cu is quite flat because the differences of their adsorption energies at the edge-bridge site and at the three-fold hollow site are below 0.2 eV. The COOH and HCOO prefer to adsorb at the top sites of two edge Cu atoms with the bidentate configuration; it is the carbonyl group in COOH and the two oxygen ends in HCOO that bind to Cu. Compared to the unsaturated species, $H_2O$, $CO_2$, and $H_2$ molecules adsorb weakly, with the binding energies typically below 0.3 eV at the Cu edge.

In parallel to the $Cu/ZrO_2$ system, we also examined the nine species (i) on the unsupported Cu strip ($Cu_{us}$) that is created by
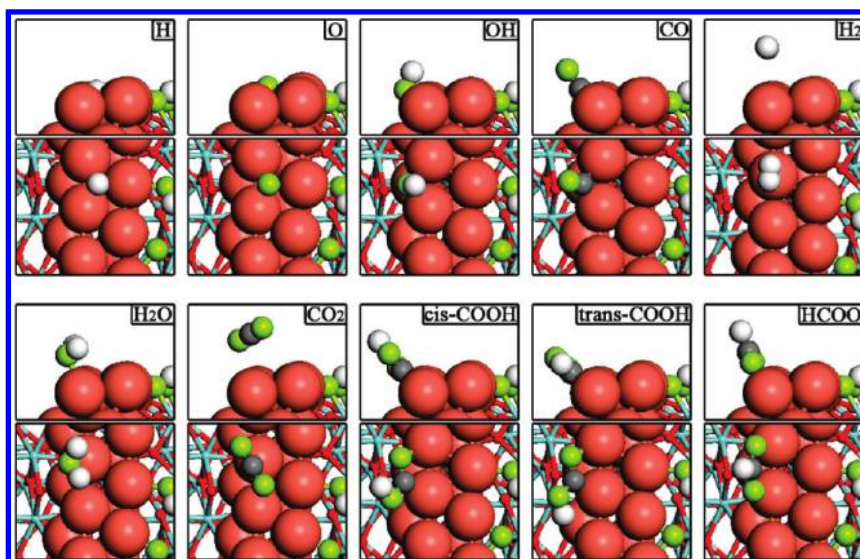
**Figure 2.** Most stable adsorption configurations for possible species involved in the WGS reaction at the Cu edge of Cu/ZrO$_2$. Upper panels, side view; lower panels, top view. H, white; C, gray; O of adsorbates, light green; lattice O, red; Cu, orange; Zr, cyan. The precovered CO spectators at the Cu edge are not shown for clarity.

simply removing the oxide support and interfacial O and OH species from Cu/ZrO$_2$ and (ii) on clean Cu(111). The adsorption energetics are compared with those in the Cu/ZrO$_2$ system in Table 1. While the adsorption sites of most species are similar, we found, interestingly, that the Cu/ZrO$_2$ system exhibits the strongest binding ability toward most of the species, while the two pure Cu substrates (Cu$_{us}$ and Cu(111)) have similar binding ability. For example, the adsorption energy of OH is 3.55 eV over Cu/ZrO$_2$ but lowers to $\sim$3.0 eV on Cu(111) and on Cu$_{us}$.

Next, we concentrated on the mechanism of the WGS reaction on Cu/ZrO$_2$ and on Cu$_{us}$. To identify the reaction network, we employed a trial-and-error iterative approach; (i) the likely reaction channels for a given intermediate were first scrutinized; (ii) guided by the calculated reaction barriers $E_a$, we only continued the low-barrier reaction channels to reach the next new intermediate and reject the too high barrier ones (e.g., the barrier larger than 2 eV); and (iii) we repeated (i) and (ii) until the target products were yielded. Following this, we identified two parallel reaction channels; one is the redox mechanism, and another is a COOH-mediated mechanism. The potential energy profiles of the two routes over the Cu/ZrO$_2$ model catalyst are displayed in Figure 3, where the same routes examined on the unsupported Cu strip are also shown for comparison. The optimized key TS structures are illustrated in Figure 4, and all of the computed barriers with ZPE correction have been listed in Table 2. Without specifically mentioning, the reported reaction heats and barriers are referenced to the initial states where the species adsorb independently, which means that the species are at infinite separation.

Both the redox and the COOH-mediated mechanisms start from H$_2$O dissociation over a top site of Cu. At the located TS of H$_2$O dissociation (TS1 in Figure 4), the breaking H–OH bond is 1.52 Å, and the O–Cu distance is 1.95 Å. The reaction barrier required is 0.76 eV with respect to the adsorbed H$_2$O. Another common elementary step in the two mechanisms is the recombination of adsorbed H atoms into H$_2$. This association reaction is endothermic by 0.43 eV and is highly activated ($E_a$ = 1.03 eV).

***3.2.1. Redox Mechanism.*** This mechanism features the surface oxygen as the oxidizing species for CO, as shown in Figure 3a. To produce O, the surface OH groups may undergo direct dissociation, which is however kinetically rather difficult at the Cu sites ($E_a$ = 1.60 eV). Instead, there is a more facile proton-transfer channel, that is, 2OH* → O* + H$_2$O* to yield atomic oxygen. The reaction is actually a nonbarrier process, and at the TS (TS2 in Figure 4), the breaking/forming O–H bonds are rather short, being 1.14/1.35 Å. This is in line with the experimental suggestion that the coupling of OH groups is predominantly responsible for surface oxygen formation.[52] Several recent DFT calculations on pure Cu surfaces have also pointed out that OH disproportionation is much preferred to its dissociation.[20−22] Once the atomic oxygen is available, CO can be oxidized on the Cu sites via CO* + O* → CO$_2$ + 2* with a barrier of 1.17 eV, which is 0.45 eV endothermic.

We also identified the redox mechanism on the unsupported Cu strip, as also shown in Figure 3a. Surprisingly, we found that the thermodynamics and the kinetics bear little similarity between the key steps on Cu$_{us}$ and those on ZrO$_2$-supported Cu. In general, H$_2$O* + * → OH* + H* and 2OH* → H$_2$O* + O* are more difficult on Cu$_{us}$, whereas the other forward steps become more facile. Specifically, without the oxide support, the H$_2$O dissociation barrier increases by 0.54 eV, while H$_2$ production barrier reduces by 0.49 eV. Similar DFT-GGA results have been reported recently for Cu(100), Cu(111), Cu(110), and Cu$_{29}$, showing that the dissociation of a single H$_2$O is indeed difficult on pure copper, with a high barrier of at least 0.93 eV.[20,21,53] The computed barrier of H$_2$ produced on Cu$_{us}$ is only half of that on Cu(111), implying that small particle size can help the H$_2$ release.[21] As these two steps are common to the redox and the COOH-mediated mechanism, such large differences in the barriers should have a significant effect on the catalytic activity, as will be addressed in section 3.3.

***3.2.2. COOH-Mediated Mechanism.*** Alternative to the atomic O, the OH species can recombine with CO to form the COOH over Cu/ZrO$_2$, as shown in Figure 3b. The CO + OH reaction is endothermic by 0.43 eV with a barrier of 0.87 eV. At the TS (TS5 in Figure 4), the nascent C–O bond is 2.07 Å, and it is 1.37 Å in the formed *cis*-COOH species. Before releasing CO$_2$, the O–H bond of the *cis*-COOH needs to rotate around its C–OH bond to form *trans*-COOH, which is a nearly thermoneutral process. The rotation barrier is computed to be 0.54 eV, close to the reported values of 0.40 and 0.52 eV on Cu(111).[21,22]
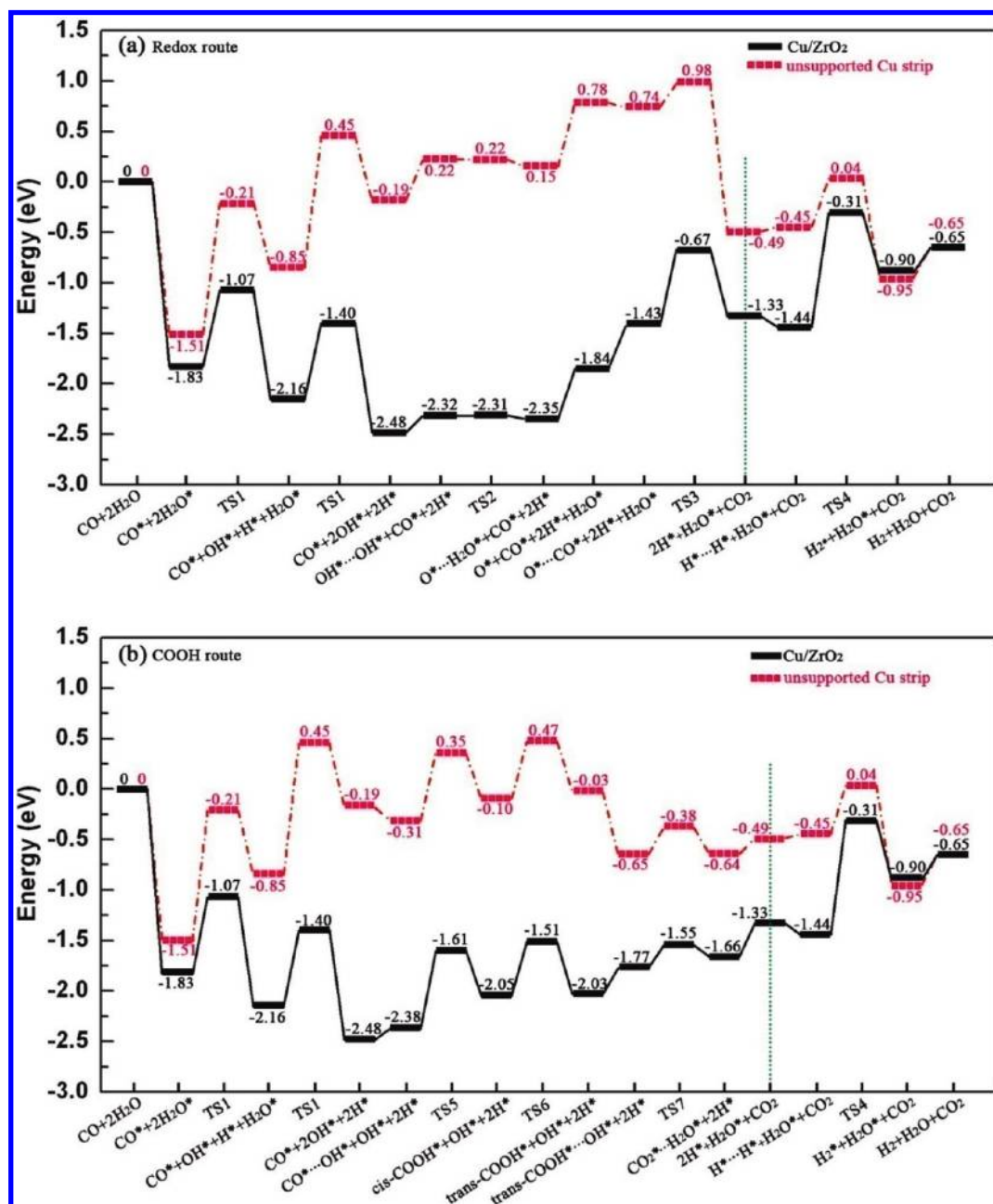
**Figure 3.** Potential energy diagrams for the WGS reaction through the (a) redox and (b) COOH-mediated routes at the Cu edge of $Cu/ZrO_2$ and on $Cu_{us}$. The "+" and "..." symbols denote the infinite separation and the coadsorption of the adsorbates, respectively. The dotted lines at the $2H^*$ + $H_2O^*$ + $CO_2$ step indicate the releasing of a $CO_2$ from the surface to the gas phase (such a process involves a dramatic gain in free energy due to the large entropy of the gas-phase molecule). The 0 on the *y*-axis is set as the sum of the energies of gaseous reactants and the bare substrate.

The direct O−H breaking of COOH is highly activated, with a barrier of 1.4 eV. Instead, the COOH decomposition to $CO_2$ is much facilitated if an adjacent OH is present. The proton transfer via $COOH^* + OH^* \rightarrow CO_2 + H_2O^* + *$ has a barrier of only 0.48 eV, which is also more facile than another proton-transfer reaction $COOH^* + O^* \rightarrow CO_2 + OH^* + *$ ($E_a = 0.99$ eV). It is worth mentioning that COOH has also been found as a key intermediate by recently published DFT calculations for the WGS reaction over $Cu_8/TiO_{2-x}(110)$ and $Ce_6O_{13}/Cu(111)$, where the copper-oxide interface was suggested to play a role in the generation of this intermediate.[5,6]

It should be pointed out that, although the formate (HCOO) species has been identified in experiment, this intermediate cannot be easily produced on the Cu sites through the direct coupling of CO and OH since the calculated barrier is more

than 2 eV. The difficulty to form HCOO directly was also reported in the previous DFT pathway on Cu(111).[21,22] We therefore suggest that formate may originate well from other secondary processes, such as the direct hydrogenation of the product $CO_2$ that was shown to occur readily at the Cu/oxide interface.[43,54]

The COOH-mediated reaction route is also feasible at the unsupported Cu strip, as also shown in Figure 3b. Similar to that in the redox mechanism, the reaction energies and barriers for the COOH-mediated mechanism are significantly modified due to the lack of the oxide support. It is noticed that the CO + OH and *trans*-COOH + OH steps are facile on the unsupported Cu with the barriers being ~0.3 eV lower than those in the $Cu/ZrO_2$ system.
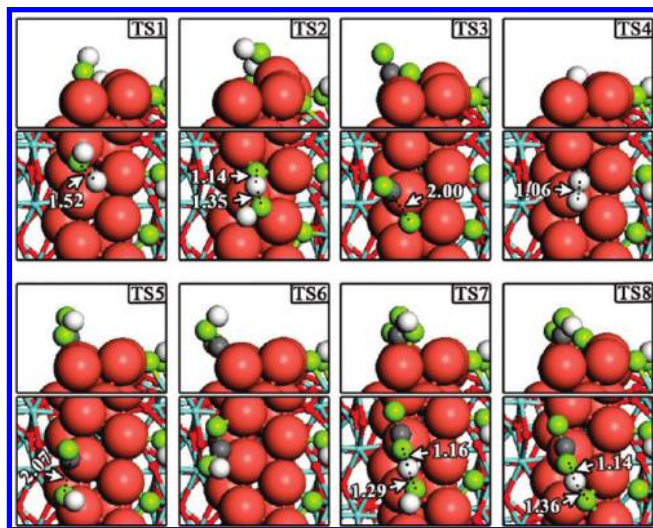
**Figure 4.** Geometrical structures of transition states identified in the WGS reaction at the Cu edge of Cu/ZrO₂. TS1 is for $H_2O^* + ^* \leftrightarrow OH^* + H^*$, TS2 for $2OH^* \leftrightarrow H_2O^* + O^*$, TS3 for $CO^* + O^* \rightarrow CO_2 + 2^*$, TS4 for $2H^* \rightarrow H_2 + 2^*$, TS5 for $CO^* + OH^* \leftrightarrow cis$-$COOH^* + ^*$, TS6 for $cis$-$COOH^* \leftrightarrow trans$-$COOH^*$, TS7 for $trans$-$COOH^* + OH^* \rightarrow CO_2 + H_2O^* + ^*$, and TS8 for $trans$-$COOH^* + O^* \rightarrow CO_2 + OH^* + ^*$. Upper panels, side view; lower panels, top view. H, white; C, gray; O of adsorbates, light green; lattice O, red; Cu, orange; Zr, cyan. The precovered CO spectators at the Cu edge are not shown for clarity.

In brief, we identified two distinct pathways for the WGS reaction over the Cu/ZrO₂ model system. By comparing the same pathways on the unsupported Cu system, we demonstrated that the thermodynamics and the kinetics of the elementary steps are sensitive to the presence of the oxide support. In the following, the effect of the oxide support will be quantitatively evaluated by microkinetic modeling.[55,56]

**3.2.3. Microkinetic Simulation of the WGS Reaction.** In order to quantitatively distinguish the two pathways and evaluate the support effect, we further performed microkinetic modeling based on the DFT-determined reaction network. The data of the reactions are shown in Table 2. According to the typical experimental conditions, we set a feed composition of 6% CO, 11% CO₂, 45% H₂, and 38% H₂O with the temperature at 503 K and the pressure at 0.15 MPa in the simulation.[2] On the basis of thermodynamic equations, the chemical potentials for gaseous H₂O and CO at the reaction condition are derived to be −0.92 and −1.06 eV with respect to their total energies at 0 K, respectively.[42] The pre-exponential factors for the adsorptions of the H₂O and CO can thus be estimated to be $6.37 \times 10^3$ and $2.52 \times 10^2 \text{ s}^{-1}$.[43] For Langmuir−Hinshelwood-type reactions, the pre-exponential factors are computed based on transition-state theory and statistical mechanics, as listed in Table 2.[57] For CO adsorption on metals, it is known that the standard DFT-GGA functionals generally overestimate the adsorption energy.[58,59] For the Cu case, Lopez and Nørskov reported that the adsorption energy can be overestimated by 0.38−0.42 eV on Cu(111).[60,61] Accordingly, we reduced $E_{ad}$(CO) down to 0.98 eV in our microkinetic modeling, which is 0.35 eV lower than the calculated DFT value. We noticed that recent studies have shown that it is now possible to utilize the results from more accurate quantum mechanics methods in small cluster calculations to correct the DFT adsorption energy of CO,[62] which is however beyond the scope of the current work.

At the achieved steady state from our microkinetic simulation, the surface is composed primarily of free sites (76%), CO (12%), H (11%), and OH (0.9%), and the coverages of other species

are below 0.03%. Our kinetic simulation did not account for the coverage of the species at the other sites. For example, formate can form well at the Cu−oxide interface (see subsection 3.2.2) and is indeed observed in experiment.[63,64] They are spectators of the WGS reaction at the Cu-only sites. Consistently, the adsorbed hydrogen was predicted by a recent DFT-parametrized microkinetic simulation of the WGS reaction on pure Cu(111) with a coverage of ∼10%.[21] The WGS reaction predominantly proceeds through the COOH mechanism because the rate of CO₂ production in this route is 116 times larger than that in the redox route. This finding agrees with the corresponding microkinetic simulation on Cu(111).[21] On the basis of Campbell's definition on the rate-determining step,[65] we have individually adjusted the barriers of the elementary steps by ±0.1 eV so as to determine which elementary step can affect mostly the rate of the WGS reaction. The largest effect occurs at the water dissociation step; the rate of the WGS reaction increases by 15 times if the barrier decreases by 0.1 eV. This is consistent with the general consensus that water dissociation is the rate-determining step on Cu-based catalysts.[12,13,17−21] More importantly, the microkinetic simulation predicts that the WGS reaction on Cu/ZrO₂ is two orders of magnitude faster than that on the unsupported Cu$_{us}$. Our results are in line with a recent kinetic experiment of the WGS reaction over Cu/TiO₂, which was measured to be 16 times more active at 573 K than Cu(111).[5] The promotion effect of ZrO₂ can be attributed to the enhanced water dissociation rate over Cu/ZrO₂ (ZPE-corrected barriers: 1.11 eV for Cu$_{us}$ and 0.55 eV for Cu/ZrO₂).

**3.3. Origin of the Oxide Support in Promoting the WGS Reaction.** We are now at the position to address why the oxide support can help to enhance water dissociation, although it does not take part in the reaction directly. From thermodynamics, we can see that the Cu sites in Cu/ZrO₂ have a larger affinity toward surface intermediates compared to the pure Cu systems Cu$_{us}$ and Cu(111) (Table 1). The final state of H₂O dissociation, OH and H, is about 0.9 eV more stable on Cu/ZrO₂ than that on the two Cu systems, while the adsorption energy of water on the three systems is no more different by 0.25 eV. As a consequence, water dissociation is exothermic by $\Delta H_r = -0.45$ eV on Cu/ZrO₂ but endothermic on Cu$_{us}$ ($\Delta H_r = 0.55$ eV) and on Cu(111) ($\Delta H_r = 0.07$ eV). According to the Bronsted−Evans−Polanyi principle[66,67] (the activation barrier is linearly correlated with the reaction energy), it is not surprising that water dissociation is much more facile on the Cu/ZrO₂ system. It is worthy to note that recent DFT studies by Rodríguez and co-workers have also concluded that water dissociation can be greatly facilitated over Cu₈/TiO$_{2−x}$(110) and Ce₆O₁₃/Cu(111).[5,6]

Obviously, it is more intriguing to answer why the Cu/ZrO₂ system can bond the electronegative intermediates (O and OH) more strongly. Considering that the Cu in the oxygen-rich Cu/ZrO₂ system is overall positively charged, it is naturally expected that the chemical state of Cu is important to the catalytic activity. To verify this, we further considered two model systems, that is, (OH)₂/Cu$_{us}$ and (OH)₅/Cu$_{us}$, to mimic the Cu/ZrO₂ system; the extra adsorbed OH on Cu$_{us}$ was added at the positions where the lattice O and OH species link with the Cu strip in the Cu/ZrO₂ system. The Bader charge analysis showed that the Cu strips of (OH)₂/Cu$_{us}$ and (OH)₅/Cu$_{us}$ are already positively charged to be +1.70 and +3.37 |e|, respectively. In Table 3, we compared the computed adsorption energy of atomic O on the Cu sites in Cu$_{us}$, (OH)₂/Cu$_{us}$, (OH)₅/Cu$_{us}$, and Cu/ZrO₂. Also shown are the charge states of Cu before and after the adsorption of O from Bader charge analysis.

**TABLE 2: DFT-Based Kinetic Parameters of 11 Elementary Steps Utilized in Microkinetic Analysis of the WGS Reaction at the Cu Edge of Cu/ZrO$_2$[a]**

| elementary steps | $E_f$ | $E_r$ | $A_0^f$ | $A_0^r$ |
|---|---|---|---|---|
| $H_2O(g) + * \leftrightarrow H_2O*$ | 0.00 | 0.25 | $6.37 \times 10^3$ | $1.05 \times 10^{13}$ |
| $H_2O* + * \leftrightarrow OH* + H*$ | 0.55 | 1.00 | $5.34 \times 10^{12}$ | $1.74 \times 10^{13}$ |
| $2OH* \leftrightarrow H_2O* \cdots O*$ | 0.08 | 0.00 | $2.06 \times 10^{12}$ | $7.45 \times 10^{12}$ |
| $H_2O* \cdots O* \leftrightarrow H_2O* + O*$ | 0.64 | 0.13 | $1.05 \times 10^{13}$ | $1.05 \times 10^{13}$ |
| $CO(g) + * \leftrightarrow CO*$ | 0.00 | 0.98[b] | $2.52 \times 10^2$ | $1.05 \times 10^{13}$ |
| $CO* + OH* \leftrightarrow cis\text{-}COOH* + *$ | 0.87 | 0.37 | $7.07 \times 10^{12}$ | $4.80 \times 10^{12}$ |
| $cis\text{-}COOH* \leftrightarrow trans\text{-}COOH*$ | 0.50 | 0.46 | $7.73 \times 10^{12}$ | $2.85 \times 10^{13}$ |
| $trans\text{-}COOH* + OH* \rightarrow CO_2(g) + H_2O* + *$ | 0.37 | c | $1.71 \times 10^{13}$ | c |
| $trans\text{-}COOH* + O* \rightarrow CO_2(g) + OH* + *$ | 0.87 | c | $4.88 \times 10^{12}$ | c |
| $CO* + O* \rightarrow CO_2(g) + 2*$ | 1.16 | c | $9.62 \times 10^{12}$ | c |
| $2H* \rightarrow H_2 + 2*$ | 0.94 | c | $6.21 \times 10^{12}$ | c |

[a] $E_f$ and $E_r$ represent the ZPE-corrected forward and reverse activation energies in units of eV, while $A_0^f$ and $A_0^r$ means the forward ($E_f$) and reverse ($E_r$) pre-exponential factors in units of S$^{-1}$. The feed composition is set as 6% CO, 11% CO$_2$, 45% H$_2$, and 38% H$_2$O at 503 K and 0.15 MPa.[2] All of the barriers are referenced to the reactants at infinite separation. [b] Considering that $E_{ad}(CO)$ is overestimated by standard GGA functionals on Cu(111),[60,61] the DFT-calculated $E_{ad}(CO)$ value is adjusted downward by 0.35 eV in microkinetics. [c] The readsorption of CO$_2$ and H$_2$ products is not considered so as to achieve the theoretical conversion with no interference of secondary reactions (namely, the product readsorption/decomposition).

**TABLE 3: Adsorption Energy of O ($E_{ad}(O)$) and Bader Charge for the O Adsorption on Various Cu Substrates[a]**

| | substrates[a] | | | | |
|---|---|---|---|---|---|
| | Cu$_{us}$ | (OH)$_2$/Cu$_{us}$ | (OH)$_5$/Cu$_{us}$ | Cu/ZrO$_2$ | Cu(111) |
| $E_{ad}(O)$, eV | 0.87 | 1.25 | 1.41 | 2.25 | 1.44 |
| $Q(O)$, \|e\| | −0.95 | −0.96 | −0.95 | −0.97 | −0.95 |
| $Q(Cu)$, \|e\| | 0.00 | 1.70 | 3.37 | 2.90 | 0.00 |
| $Q(Cu^{ads})$, \|e\| | 1.52 | 2.62 | 4.31 | 4.54 | 0.95 |

[a] $E_{ad}(O)$ is calculated with respect to 1/2 O$_2$ in the gas phase. $Q(Cu)$ and $Q(Cu^{ads})$ are for the Bader charges of Cu substrates before and after the adsorption of an O atom.

Table 3 shows that the net charge of adsorbed oxygen, $Q(O)$, is nearly constant, ∼−0.95 \|e\| on all of the systems investigated, implying that the charge donation from Cu to O is highly efficient and is not sensitive to the Cu forms. By comparing the three Cu$_{us}$ systems, we noticed that the increase of the charge on Cu can indeed enhance the adsorption of O. The adsorption energy of O, $E_{ad}(O)$, is 0.87 eV on the Cu$_{us}$, and it increases to 1.25 and 1.41 eV on the (OH)$_2$/Cu$_{us}$, and (OH)$_5$/Cu$_{us}$, respectively. Considering that the adsorbed O atom is highly negatively charged, it is reasonable from electrostatic interaction that the higher the cationic charge on Cu is, the stronger the bonding ability to the O atom will be. Apart from the charging effect, it is also noticed that the adsorption energy of O on Cu(111) (Cu: nine coordination) is larger than that on Cu$_{us}$ strip (Cu: six coordination). This implies that the adsorption of O prefers a high coordination environment on neutral Cu systems where the surface electron density is high, in line with the strong ionic bonding character of O on Cu.

Next, we turn to the Cu/ZrO$_2$ model system where the Cu charge initially is not the highest (2.90 \|e\|). Interestingly, we find that the adsorption of O has induced further electrons to flow from Cu to ZrO$_2$, leading to the strongest positively charged Cu (4.54 \|e\|), and consistently, $E_{ad}(O)$ is the highest on Cu/ZrO$_2$. It implies that ZrO$_2$ can act as a buffer to accept/release electrons from/to Cu during the catalytic reaction, which not only stabilizes the dispersed Cu but also boosts the catalytic activity. The picture described here confirmed that the enhanced adsorption energy of O on Cu can be partly rationalized by electrostatic interaction, although the contributions from other synergetic effects in the composite, including the structural relaxation and the associated covalent bonding, cannot be fully ruled out.

## 4. Conclusion

The water−gas shift reaction over a binary model Cu/ZrO$_2$ catalyst has been investigated by first-principles calculations and microkinetic modeling, with the aim to elucidate the catalytic role of oxide supports. We found that the ZrO$_2$ does not directly take part in the WGS reaction because H$_2$O dissociates too facilely at the interfacial sites and the interfacial oxidative species such as O and OH cannot be easily removed by CO at reaction conditions.

In the oxygen-rich Cu/ZrO$_2$ system, we show that the COOH-mediated reaction pathway is preferred over the redox pathway, and the H$_2$O dissociation is the rate-determining step. By comparing the WGS activity on the unsupported Cu strips and on Cu(111), we conclude that the ZrO$_2$ oxide support can indeed promote the WGS reactivity. The positively charged Cu sites in the vicinity of the Cu/ZrO$_2$ interfaces are the most active sites, where the barrier of H$_2$O dissociation is only 0.55 eV, about half of that in pure Cu systems. The physical origin is identified as the enhanced electrostatic interaction between the positively charged Cu sites and the electronegative adsorbates such as O and OH species. The atomic-level knowledge on the composite Cu-oxide system obtained here provides important clues on the development of a better WGS catalyst.

**References and Notes**

(1) Huber, F.; Venvik, H.; Rønning, M.; Walmsley, J.; Holmen, A. *Chem. Eng. J.* **2008**, *137*, 686.

(2) Saito, M.; Murata, K. *Catal. Surv. Asia* **2004**, *8*, 285.

(3) Rodriguez, J. A.; Liu, P.; Hrbek, J.; Evans, J.; Pérez, M. *Angew. Chem., Int. Ed.* **2007**, *46*, 1329.

(4) Liu, X.-M.; Lu, G.-Q.; Yan, Z.-F.; Beltramini, J. *Ind. Eng. Chem. Res.* **2003**, *42*, 6518.

(5) Rodríguez, J. A.; Evans, J.; Graciani, J.; Park, J.-B.; Liu, P.; Hrbek, J.; Sanz, J. F. *J. Phys. Chem. C* **2009**, *113*, 7364.

(6) Rodríguez, J. A.; Graciani, J.; Evans, J.; Park, J.-B.; Yang, F.; Stacchiola, D.; Senanayake, S. D.; Ma, S.; Pérez, M.; Liu, P.; Sanz, J. F.; Hrbek, J. *Angew. Chem., Int. Ed.* **2009**, *48*, 8047.

(7) Rodríguez, J. A.; Liu, P.; Wang, X.; Wen, W.; Hanson, J.; Hrbek, J.; Pérez, M.; Evans, J. *Catal. Today* **2009**, *143*, 45.

(8) Hayek, K.; Kramer, R.; Paál, Z. *Appl. Catal., A* **1997**, *162*, 1.

(9) Sun, Y.; Sermon, P. A. *Catal. Lett.* **1994**, *29*, 361.

(10) Rhodes, C.; Hutching, G. H.; Ward, A. M. *Catal. Today* **1995**, *23*, 43.

(11) Koryabkina, N. A.; Phatak, A. A.; Ruettinger, W. F.; Farrauto, R. J.; Ribeiro, F. H. *J. Catal.* **2003**, *217*, 233.

(12) Fishtik, I.; Datta, R. *Surf. Sci.* **2002**, *512*, 229.

(13) Callaghan, C.; Fishtik, I.; Datta, R.; Carpenter, M.; Chmielewski, M.; Lugo, A. *Surf. Sci.* **2003**, *541*, 21.

(14) Callaghan, C. A.; Vilekar, S. A.; Fishtik, I.; Datta, R. *Appl. Catal., A* **2008**, *345*, 213.

(15) Ko, J. B.; Bae, C. M.; Jung, Y. S.; Kim, D. H. *Catal. Lett.* **2005**, *105*, 157.

(16) Águila, G.; Guerrero, S.; Araya, P. *Catal. Commun.* **2008**, *9*, 2550.

(17) Nakamura, J.; Campbell, J. M.; Campbell, C. T. *J. Chem. Soc., Faraday Trans.* **1990**, *86*, 2725.

(18) Campbell, C. T.; Daube, K. A. *J. Catal.* **1987**, *104*, 109.

(19) Spencer, M. S. *Top. Catal.* **1999**, *8*, 259.

(20) Liu, P.; Rodríguez, J. A. *J. Chem. Phys.* **2007**, *126*, 164705.

(21) Gokhale, A. A.; Dumesic, J. A.; Mavrikakis, M. *J. Am. Chem. Soc.* **2008**, *130*, 1402.

(22) Tang, Q.-L.; Chen, Z.-X.; He, X. *Surf. Sci.* **2009**, *603*, 2138.

(23) Campbell, C. T.; Koel, B. E.; Daube, K. A. *J. Vac. Sci. Technol., A* **1987**, *5*, 810.

(24) Wen, W.; Jing, L.; White, M. G.; Marinkovic, N.; Hanson, J. C.; Rodríguez, J. A. *Catal. Lett.* **2007**, *113*, 1.

(25) Wang, X.; Rodríguez, J. A.; Hanson, J. C.; Gamarra, D.; Martínez-Arias, A.; Fernández-García, M. *Top. Catal.* **2008**, *49*, 81.

(26) Li, L.; Zhan, Y.; Zheng, Q.; Zheng, Y.; Lin, X.; Li, D.; Zhu, J. *Catal. Lett.* **2007**, *118*, 91.

(27) Chinchen, G. C.; Spencer, M. S.; Waugh, K. C.; Whan, D. A. *J. Chem. Soc., Faraday Trans.* **1987**, *83*, 2193.

(28) Ovesen, C. V.; Clausen, B. S.; Hammershøi, B. S.; Steffensen, G.; Askgaard, T.; Chorkendorff, I.; Nørskov, J. K.; Rasmussen, P. B.; Stoltze, P.; Taylor, P. *J. Catal.* **1996**, *158*, 170.

(29) Rodríguez, J. A.; Hanson, J. C.; Wen, W.; Wang, X.; Brito, J. L.; Martínez-Arias, A.; Fernández-García, M. *Catal. Today* **2009**, *145*, 188.

(30) Clausen, B. S.; Steffensen, G.; Fabius, B.; Villadsen, J.; Feidenhanúl, R.; Topsøe, H. *J. Catal.* **1991**, *132*, 524.

(31) Saito, M.; Tomoda, K.; Takahara, I.; Murata, K.; Inaba, M. *Catal. Lett.* **2003**, *89*, 11.

(32) Tabakova, T.; Idakiev, V.; Papavasiliou, J.; Avgouropoulos, G.; Ioannides, T. *Catal. Commun.* **2007**, *8*, 101.

(33) Shishido, T.; Yamamoto, M.; Li, D.; Tian, Y.; Morioka, H.; Honda, M.; Sano, T.; Takehira, K. *Appl. Catal., A* **2006**, *303*, 62.

(34) Kumar, P.; Idem, R. *Energy Fuels* **2007**, *21*, 522.

(35) Garbassi, F.; Petrini, G. *J. Catal.* **1984**, *90*, 106.

(36) Soler, J. M.; Artacho, E.; Gale, J. D.; García, A.; Junquera, J.; Ordejón, P.; Sánchez-Portal, D. *J. Phys.: Condens. Matter* **2002**, *14*, 2745.

(37) Perdew, J. P.; Burke, K.; Ernzerhof, M. *Phys. Rev. Lett.* **1996**, *77*, 3865.

(38) Troullier, N.; Martins, J. L. *Phys. Rev. B* **1991**, *43*, 1993.

(39) Artacho, E.; Sánchez-Portal, D.; Ordejón, P.; García, A.; Soler, J. M. *Phys. Status Solidi B* **1999**, *215*, 809.

(40) Monkhorst, H. J.; Pack, J. D. *Phys. Rev. B* **1976**, *13*, 5188.

(41) Wang, H.-F.; Liu, Z.-P. *J. Am. Chem. Soc.* **2008**, *130*, 10996.

(42) *CRC Handbook of Chemistry and Physics*, 84th ed.; CRC Press: Boca Raton, FL, 2003−2004.

(43) Tang, Q.-L.; Hong, Q.-J.; Liu, Z.-P. *J. Catal.* **2009**, *263*, 114.

(44) Christensen, A.; Carter, E. A. *Phys. Rev. B* **1998**, *58*, 8050.

(45) Wang, C.-M.; Fan, K.-N.; Liu, Z.-P. *J. Am. Chem. Soc.* **2007**, *129*, 2642.

(46) Mattos, L. V.; Noronha, F. B. *J. Power Sources* **2005**, *145*, 10.

(47) Alfonso, D. R.; Jaffe, J. E.; Hess, A. C.; Gutowski, M. *Phys. Rev. B* **2003**, *68*, 155411.

(48) Taek, K.; Bell, A. T. *Catal. Lett.* **2002**, *80*, 63.

(49) Liu, Z.-P.; Gong, X.-Q.; Kohanoff, J.; Sanchez, C.; Hu, P. *Phys. Rev. Lett.* **2003**, *91*, 266102.

(50) Henkelman, G.; A., A.; Jónsson, H. *Comput. Mater. Sci.* **2006**, *36*, 354.

(51) Bader, R. F. W. *Acc. Chem. Res.* **1985**, *18*, 9.

(52) Henderson, M. A. *Surf. Sci. Rep.* **2002**, *46*, 1.

(53) Tang, Q.-L.; Chen, Z.-X. *J. Chem. Phys.* **2007**, *127*, 104707.

(54) Wambach, J.; Baiker, A.; Wokaun, A. *Phys. Chem. Chem. Phys.* **1999**, *1*, 5071.

(55) Stoltze, P.; Nørskov, J. K. *Phys. Rev. Lett.* **1985**, *55*, 2502.

(56) Stoltze, P.; Nørskov, J. K. *J. Catal.* **1988**, *110*, 1.

(57) Wynne-Jones, W. F. K.; Eyring, H. *J. Chem. Phys.* **1935**, *3*, 492.

(58) Hammer, B.; Morikawa, Y.; Nørskov, J. K. *Phys. Rev. Lett.* **1996**, *76*, 2141.

(59) Brown, W. A.; Kose, R.; King, D. A. *Chem. Rev.* **1998**, *98*, 797.

(60) Lopez, N.; Nørskov, J. K. *Surf. Sci.* **2001**, *477*, 59.

(61) Kirstein, W.; Krüger, B.; Thieme, F. *Surf. Sci.* **1986**, *176*, 505.

(62) Ren, X.; Rinke, P.; Scheffler, M. *Phys. Rev. B* **2009**, *80*, 045402.

(63) Schild, C.; Wokaun, A.; Baiker, A. *J. Mol. Catal.* **1990**, *63*, 243.

(64) Borodko, Y.; Somorjai, G. A. *Appl. Catal., A* **1999**, *186*, 355.

(65) Campbell, C. T. *J. Catal.* **2001**, *204*, 520.

(66) Brønsted, N. *Chem. Rev.* **1928**, *5*, 231.

(67) Evans, M. G.; Polanyi, N. P. *Trans. Faraday Soc.* **1936**, *32*, 1333.